Desalination and Water Treatment
www.deswater.com
doi: 10.5004/dwt.2018.22992

133 (2018) 227–236
November

Facial synthesis of dual applicable $ZnFe_2O_4$@CuS nanohybrid: catalytic reduction of nitroarene and adsorption of methylene blue

Hassan Alijani[a], Mostafa Hossein Beyki[b], Reyhaneh Kaveh[c], Yousef Fazli[d,*]

[a]*Department of Chemistry, Faculty of Science, Shahid Chamran University of Ahvaz, Ahvaz, Iran, email: Alijani.hassan89@gmail.com*
[b]*School of Chemistry, University College of Science, University of Tehran, Tehran, Iran, email: hosseinbakim@gmail.com*
[c]*Chemistry Department, Sharif University of Technology, Tehran, Iran, email: reyhanehkaveh@yahoo.com*
[d]*Department of Chemistry, Amirkabir University of Technology (Tehran Polytechnic), Tehran, Iran, email: youseffazli88@gmail.com*

Received 17 February 2018; Accepted 18 August 2018

ABSTRACT

Magnetic $ZnFe_2O_4$@CuS core-shell nanostructures have been prepared by a facial polyol route. The catalytic activity of the $ZnFe_2O_4$@CuS-$NaBH_4$ system for reduction of nitro – compound in water-ethanol solution (2:1 V/V), showed that the reaction proceeds within 3 min at 60°C. A dye adsorption property of the nanostructure was also investigated with the aid of response surface methodology. Results indicate that the adsorption process is fast as equilibrium obtained within 10 min and adsorption followed the Freundlich model with a maximum capacity of 26 mg g^{-1}. Regeneration study showed that adsorbed methylene blue released with methanol-acetone solution.

Keywords: Copper sulfide; Magnetic nanostructure; Nitro reduction; Adsorption; Methylene blue

1. Introduction

In recent decades, semiconductor metal chalcogenides have attracted considerable interest owing to their excellent characteristics. Among the semiconductors, metal sulfides possess unusual physical and chemical properties such as harmlessness to the environment and capability to utilize solar energy [1,2]. Moreover, they possess superb luminescent and photochemical properties, which made them a promising candidate as photocatalysts [3–5]. Among the metal sulfides semiconductors, copper sulfide as self-doped *p*-type semiconductor possesses covalent S–S bonds with stacked layer structure [6–9]. Owing to their large surface area to the volume ratio, copper sulfide shows excellent catalytic activity in organic transformations including Biginelli reaction, coupling reaction, and synthesis of xanthenes [10–12].

Reduction of nitroaromatic compounds to their corresponding arylamines is an important organic transformation for the synthesis of various pharmaceuticals, heterocyclic compounds, dyes, and other industrially related compounds [13–15]. Over the last decade, the nitroreduction has been catalyzed with several metals, including iron, cobalt, zinc, and tin. However, the methods possess many advantages but some drawbacks such as the formation of harmful azo and azoxy-derivatives, difficulty in separating and recovering of catalyst from the reaction systems, and the requirement of a strongly acidic or basic medium that is not compatible with many organic functionalities, restricts their applications. Hydrogenation in the presence of a homogeneous or heterogeneous catalyst such as incorporated magnetic nanoparticles (MNPs) with palladium, silver, and gold is other most common methods for aromatic amine synthesis [16–20]. Although these techniques possess some advantages but preparation of coated materials with the mentioned nanoparticles is not economical as a result exploring new catalytic systems for nitro transformations is an ongoing research topic. There are some reports in the literature about using copper compounds for nitro reduction. Yoo and Lee [21] used sodium borohydride–copper sulfate system for nitro reduction but are not reusable. Moreover, Pina et al. [22] employed transition metal sulfides for this purpose. However, they found

* Corresponding author.

only marginal conversion by sodium borohydride–CuS system. Employment of the CuS for environmental remediation is another interesting area [23]. Despite the worthiness of CuS nanoparticles, they possess some drawbacks in practical application especially time-consuming manipulation from reaction media by centrifugation or filtration. Magnetic material in which the desired compound is anchored on MNPs allows the manipulation to be faster and simpler [24]. Among MNPs, ceramic ferrites especially $ZnFe_2O_4$ have been investigated in recent years for their chemical and corrosive stability as well as low saturation magnetization properties resulting expedite dispersion in aqueous solution and shorter equilibrium time [25–27].

Based on these viewpoints, $ZnFe_2O_4$ nanoparticles were synthesized by solid-state combustion method and employed as a magnetic core to prepare $ZnFe_2O_4$@CuS nanocomposite using a fast and facial polyol route. The nanohybrid has been employed for the fast reduction of nitroaniline as a versatile chemical intermediate in the preparation of dyes, pigments, and pharmaceuticals [28,29]. Furthermore, the prepared composite was utilized for the efficient adsorption of methylene blue (MB) as a model compound for removing dyes and organic contaminants from aqueous solutions. In fact, MB has wide applications and exerts some harmful effects on human beings hence, it is necessary to remove MB from aqueous solution [30–37]. Prepared nanocomposite possesses superparamagnetic property hence, can be easily manipulated under the influence of an external magnetic field. Moreover, effective parameters on dye adsorption were optimized with response surface methodology (RSM).

2. Experimental

2.1. Material and instruments

All the reagents used in this study were used as received without further purification. $Fe(NO_3)_3{\cdot}9H_2O$, $Zn(NO_3)_2{\cdot}6H_2O$, $CuSO_4$, ethylene glycol (EG), cellulose, and $Na_2S_2O_3$ were obtained from Merck (Darmstadt, Germany). Standard solutions of MB (1,000 mg L^{-1}) were prepared by dissolving the powder in the appropriate volume of distilled water. The pH adjustment was performed with 0.1 mol L^{-1} of HCl and 0.1 mol L^{-1} of NH_3. The prepared particles were characterized by powder X-ray diffraction (XRD) analysis using a Phillips powder diffractometer, X′ Pert MPD, with Cu-Ka (λ = 1.540589 Å) radiation. Field emission scanning electron microscopy (FESEM) analysis was carried out using a HITACHI S 4160. Magnetization measurements were recorded using a vibration sample magnetometer (VSM) (Lake Shore Model 7400, Japan). A Lambda-25 UV-vis spectrophotometer was used for recording the progress of the catalytic reaction and dye adsorption properties. A digital pH-meter (model 692, metrohm, Herisau, Switzerland) was used for pH adjustments.

2.2. Synthesis of $ZnFe_2O_4$@CuS nanocomposite

The $ZnFe_2O_4$ nanoparticles have been synthesized by solid-state combustion route using cellulose as fuel. About 4 mmol of Fe^{3+} and 2 mmol of Zn^{2+} have been mixed with 1.0 g of microcrystalline cellulose for 10 min then has been combusted at 150°C. Thereinafter, the gray mass was further heated at 400°C for 1 h. Magnetic $ZnFe_2O_4$@CuS was synthesized by refluxing polyol route. About 0.5 g of the nanoparticles has been dispersed in 20 mL of EG at 120°C and followed with the addition of 0.8 g of $CuSO_4$. After complete dissolving of the copper salt, 1.9 g of $Na_2S_2O_3$ in 20 mL of EG poured into the suspension and the mixture was refluxed at 140°C for 90 min. Obtained product has been washed with ethanol and distilled water and dried at 80°C for 5 h.

2.3. Typical catalytic run

To investigate the catalytic activity of the material, 10 mg of P-nitroaniline was dissolved in 5 mL of ethanol. 10 mL of distilled water and 50 mg of the catalyst were added to the solution and sonicated for 1 min. After the addition of 50 mg of $NaBH_4$, the mixture has been heated at 70°C for 3 min then, the catalyst has been collected with external magnetic field and supernatant was analyzed with UV-vis spectrophotometer. To attain solid product, after separation of the catalyst, the solution was poured in 5 mL of $CHCl_3$ and extracted with separation funnel. After evaporation of the solvent with rotary, the white crude product has been collected (melting point 138°C–140°C).

2.4. Dye adsorption procedure

Dye adsorption experiment has been performed with the batch method. As a typical run, 10 mL of MB solution at a pH of 8, with an initial concentration of 5–60 mg L^{-1} and 20 mg of the adsorbent, was shacked for 10 min. After equilibrium time, the adsorbent was separated by external magnetic field and concentration of MB in the supernatant was determined with UV-vis spectrometer. The adsorption amount was calculated based on the difference of the MB concentration in the aqueous solution before and after adsorption, according to the following equation:

$$Q = \left(C_0 - C_e\right) \times \frac{V}{W_0} \tag{1}$$

where C_0 and C_e are the initial and equilibrium concentration of MB in mg/L, V is the volume of MB solution in L, and W_0 is the weight of the composite used in g [38].

3. Results and discussions

3.1. Characterization of the material

3.1.1. XRD analysis

Typical XRD pattern of the $ZnFe_2O_4$ and the nanocomposite was shown in Fig. 1(a). In the pattern of ferrite, characteristic peaks show scattering at 2θ°= 29.64, 35.48, 35.7, 44.2, 52.72, 56.2, 61.76, and 75.1 (JCPDS No. 34-425) corresponding to (220), (311), (222), (400), (422), (511), (440), and (535) planes of zinc-ferrite structure [39]. No diffraction peaks other than those from Fe_2O_3 were obtained, indicating the high purity of the as-synthesized products. The XRD pattern of $ZnFe_2O_4$@CuS showed some changes relative to pure ferrite. The appearance of new reflections can be indexed with hexagonal CuS, which is consistent with the standard card

JCPDS No. 65-3556. Under the polyol conditions, the following reactions may occur [40,41]:

$$EG \rightarrow CH_3CHO + H_2O \quad (2)$$

$$S_2O_3^{2-} + 6CH_3CHO \rightarrow S^{2-} + S + 3CH_3CO - OCCH_3 + 3H_2O \quad (3)$$

$$S + 2CH_3CHO \rightarrow S^{2-} + CH_3CO - OCCH_3 + 2H^+ \quad (4)$$

$$S_2O_3^{2-} + H_2O \rightarrow SO_4^{2-} + H_2S \quad (5)$$

$$Cu^{2+} + H_2S \rightarrow CuS\downarrow + 2H^+ \quad (6)$$

$$Cu^{2+} + S^{2-} \rightarrow CuS\downarrow \quad (7)$$

In brief, EG dehydrates at high temperatures cause acetaldehyde formation as a reducing agent which produces S^{2-}, as shown in reactions (2) and (3). Then Cu^{2+} reacts with S^{-2} to form CuS. Moreover, released H_2S from thiosulfate–H_2O reaction reacts with copper ions and produces CuS precipitate.

Fig. 1(b) showed the magnetic hysteresis loop of the $ZnFe_2O_4$ and the synthesized $ZnFe_2O_4$@CuS (magnetic field of ±10°kOe at 25°C). The saturation magnetization of the $ZnFe_2O_4$ sample and nanocomposite is 15.04 and 5.16 emu g^{-1}, respectively. The lower saturation magnetization of the nanocomposite relative to naked ferrite is due to the low density of $ZnFe_2O_4$ in the nanocomposite structure or presence of CuS as a dead magnetic layer.

The FESEM image of $ZnFe_2O_4$ in Fig. 1(c) showed that ferrite is spherical nanoparticles with a mean size of 40 nm. This morphology is as a result of the isotopic nucleation at the interface between the nanoparticles [42]. The FESEM

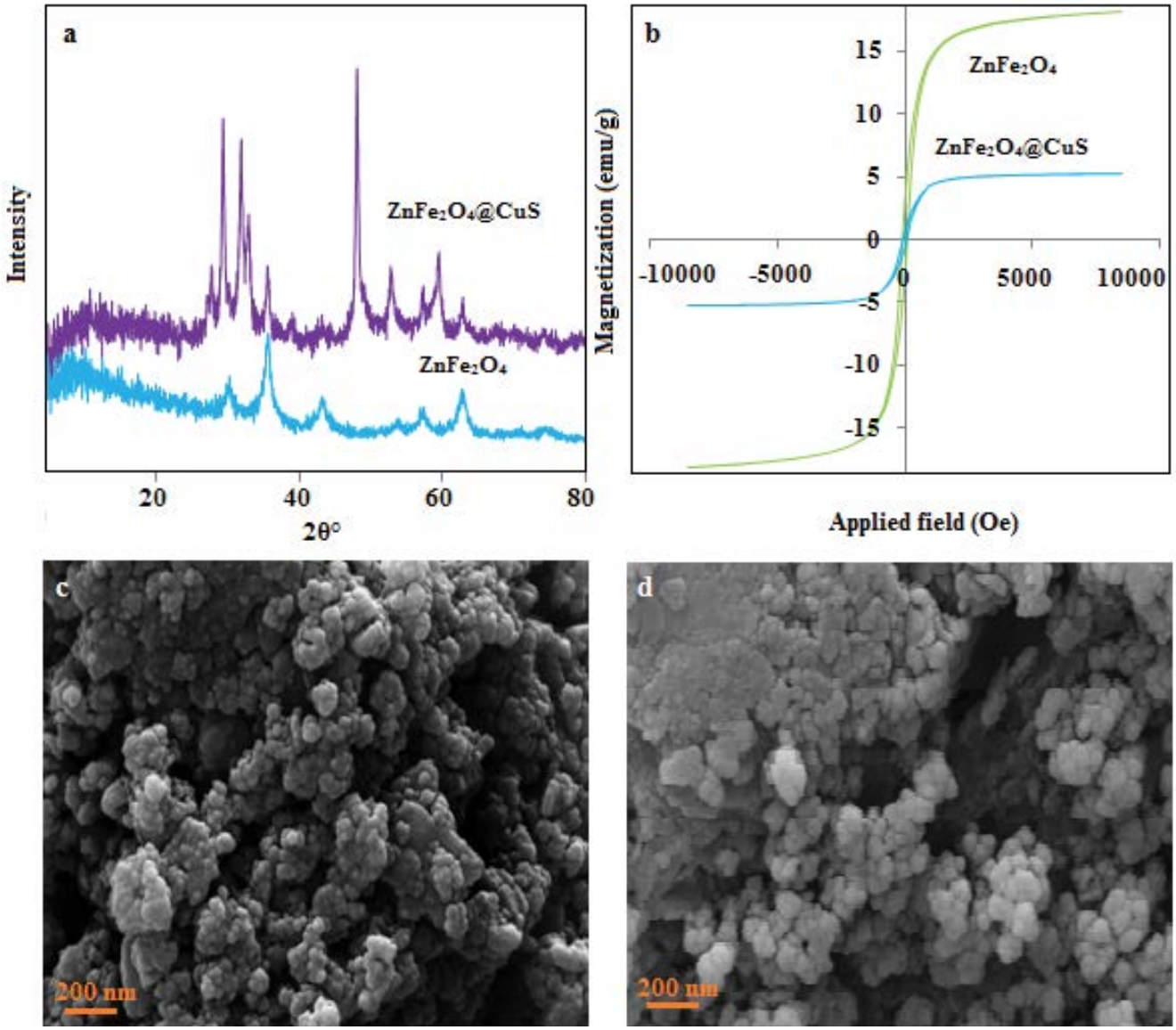

Fig. 1. The XRD pattern (a) VSM graph (b), FESEM image of ferrite (c), and composite (d).

image of $ZnFe_2O_4$@CuS in Fig. 1(d) showed the assembly of spherical particles composed of fine nanoparticles. By employment of the ferrite nanoparticles as core particles, the nanocomposite with diameters of around 50–100 nm was obtained. At the synthetic process Cu^{2+} coordinate with EG and precipitated as nuclei on the ferrite surface which continued with aggregation of the primary CuS nanocrystals form larger secondary particles at high temperature [43].

3.2. Catalytic performances of the nanocomposite

UV-vis spectroscopy was employed to monitor the catalytic performances of nanohybrid. Fig. 2 represents the absorbance of nitroaniline before and after the catalytic reaction. It can be seen that after the catalytic reaction, the peak for nitroaniline at 380 nm disappeared and a new peak corresponding to phenylenediamine appeared at 303 nm. To investigate the efficiency of the catalytic system, performances of $NaBH_4$, $ZnFe_2O_4$, CuS, and $ZnFe_2O_4$@CuS in the presence or absence of $NaBH_4$ were also examined (Table 1). The results indicate that in the presence of ferrite,

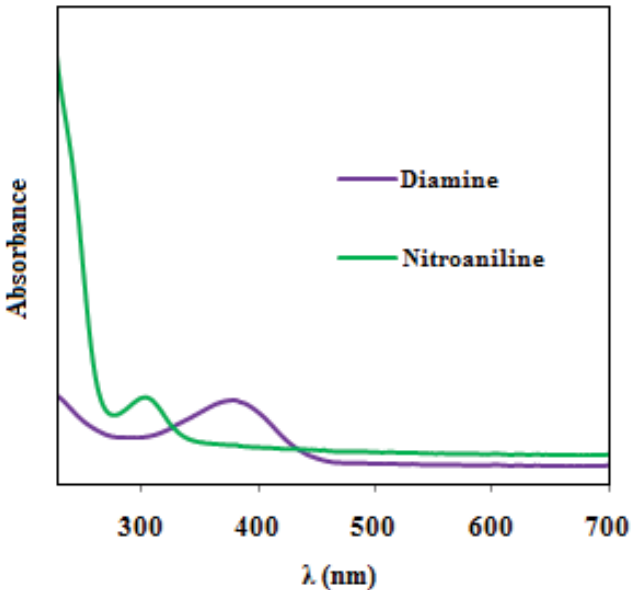

Fig. 2. A typical UV-vis spectra of the nitro compound before and after catalytic reduction.

no conversion has occurred. Moreover, ferrite-$NaBH_4$ system showed only 9% conversion as well as it was reached to about 12%, 22%, and 28% in CuS-$NaBH_4$ system with 3, 10, and 15 mol ratio of $NaBH_4$/nitroaniline, respectively. The conversion in the $ZnFe_2O_4$@CuS system in the absence of $NaBH_4$ is also low; however, the addition of $NaBH_4$ promotes reaction up to complete conversion. It was observed that amount of $NaBH_4$ has the main effect on the reaction as in 3:1 mol ratio of $NaBH_4$/nitroaniline (T = 60°C) reaction proceed within 30 min as well as it was completed after 10 min at 10:1 ratio. It was found that the reaction has been completed within 3 min at 15:1 mol ratio of $NaBH_4$/nitroaniline in the $ZnFe_2O_4$@CuS catalytic system. These results prove the necessity of three fragments, that is, $ZnFe_2O_4$, $NaBH_4$, and CuS for complete reduction of the nitro compound. $NaBH_4$ is the main component for a nitro reduction since it releases hydrogen in aqueous solution at high temperatures or in the presence of metal catalysts [44,45]. However, the reaction system contains $ZnFe_2O_4$ as a metal fragment, but it seems that it cannot exert an effective role on hydrolysis of $NaBH_4$, which may be owing to the coating of the nanoparticles surface with the copper sulfide. According to the results, fast proceed of the reaction needs rising the temperature up to 60°C hence, it can be concluded that this situation is in favor of $NaBH_4$ hydrolysis. Copper sulfide is another active fragment in this reaction. It is known that polysulfide compounds, $S_2O_4^{2-}$ and sodium sulfide can reduce nitro compounds hence it can be estimated that CuS also has potential to reduce nitro groups like to the conventional sulfide compounds. Presence of H_2O is also a main factor for this reaction. Results showed that an increase in water concentration causes a decrease in the reduction of time as the volume of distilled water raised from 5 to 10 mL the reduction time decreased from 10 to 3 min. This can be owing to the more effective hydrolysis of $NaBH_4$ at higher concentration of water which causes faster generation of hydrogen for nitro reduction. The proposed reaction is schematically shown in Fig. 3.

3.3. Optimizing dye adsorption variants

RSM was employed to optimize effective parameters on MB adsorption. For this purpose Box–Behnken design was used to run adsorption experiments by Design Expert software version, 7.0.0. The performed design including three factors (pH: *A*, contact time: *B*, and adsorbent dose: *C*) at three levels (−1, 0, and +1) with total 17 runs, 1 block, and

Table 1
Comparing the role of catalyst components in nitroaniline conversion

	Without $NaBH_4$	$NaBH_4$/nitroaniline (3)[a]	$NaBH_4$/nitroaniline (10)[a]	$NaBH_4$/nitroaniline (15)[a]
$ZnFe_2O_4$	–	9	12	15
$NaBH_4$	–	10	16	22
CuS	5	12	22	28
$ZnFe_2O_4$ – CuS	10	99[b]	99[c]	99[d]

[a]Mol ratio.
[b]After 30 min.
[c]After 10 min.
[d]After 3 min.

5 center point. The validity of the equations was examined by the analysis of variance (ANOVA). Moreover, to overview the variables effects and optimum level of them 3D response surface plots were drawn. A polynomial equation was used for the prediction of response as a function of independent variables and their interactions [Eq. (8)]:

$$Y = \beta_0 + \sum_{i=1}^{k} \beta_i X_i + \sum_{i=1}^{k} \beta_{ii} X_i^2 + \sum_{i=1}^{k-1} \sum_{j=2}^{k} \beta_{ij} X_i X_{ij} \quad (8)$$

where Y is the predicted response; X_i and X_j represent the coded values of independent variables, and β is the regression coefficient constant of the developed model [46,47]. The relationship between removal percentage (R%) and variables was shown in Eq. (9).

$$\text{Removal} = +83.88 - 2.13A + 4.75B + 20.13C + 3.00AB + 1.75AC - 2.50BC + 7.18A^2 - 1.07B^2 - 10.32C^2 \quad (9)$$

The significance of coefficients was determined from F and P values based on the ANOVA calculation in Table 2. Results depicted the P values of <0.0001 with an F value of 32.05 and confirmed that adsorption is significant. Moreover, it can be seen that adsorption is independent of pH, however, shacking time and adsorbent dosage are effective parameters on dye adsorption. Fig. 4(a) shows the normal probability plot as a straight line and low violation of the assumptions underlying the analyses confirms the normality of the data. Fig. 4(b) shows that the response points are located in a narrow range with a low value of standard deviation (3.8) between the experimental and predicted results. Moreover, the R^2 value of 0.97 is in good agreement with adjusted R^2 (0.94) indicated a high dependence and correlation between the observed and the predicted values of response. Adequate precision (the signal to noise ratio) was 19.24 demonstrated that model is significant for the MB adsorption. According to perturbation plot (Fig. 4(c)), a steep curvature in time and dosage curve shows that the response of adsorption was sensitive to these factors. The relatively flat line of the pH shows slightly sensitivity of the responses to change in this component.

According to the results of 3D plots (Fig. 5), the optimum value of 8 was obtained for pH. Moreover, the optimum value of contact time and adsorbent dosages is 10 min and 20 mg, respectively. To evaluate the accuracy of the predicted removal percentage (100.3%) at the optimum value of parameters, three experiments were carried out and results showed a good agreement between the optimum-calculated response and mean experimental response (97%).

According to results at the pH of 8.0 maximum removals efficiency was obtained. At this situation, hydrogen bonds because of the functional groups on the sorbent surfaces (S, OH) participate in MB adsorption. Electrostatic interaction between the cationic dye and sorbent surface is another main mechanism since zinc ferrite and CuS have a negative charge at the working pH [48,49]. Morphology of the sorbent has also the main role in the adsorption process. According to the FESEM image, as synthesized nanocomposite generate pore areas between the fragments that are ready to adsorb MB.

3.3.1. Isotherm study

In Fig. 6(a), the results of the equilibrium adsorption isotherm in the concentration range of 5–60 mg L^{-1} at optimum conditions (pH = 8, time 10 min, and adsorbent dosage of 20 mg) are presented. The sorption is approximately complete with 5–20 mg L^{-1} of MB and reached 88% at an initial concentration of 60 mg L^{-1}. These results confirmed high efficiency of the $ZnFe_2O_4$-CuS for the adsorption of cationic dye from an aqueous solution. The effect of concentration was also analyzed in terms of Langmuir and Freundlich models. The equation for the Freundlich model that suggests the

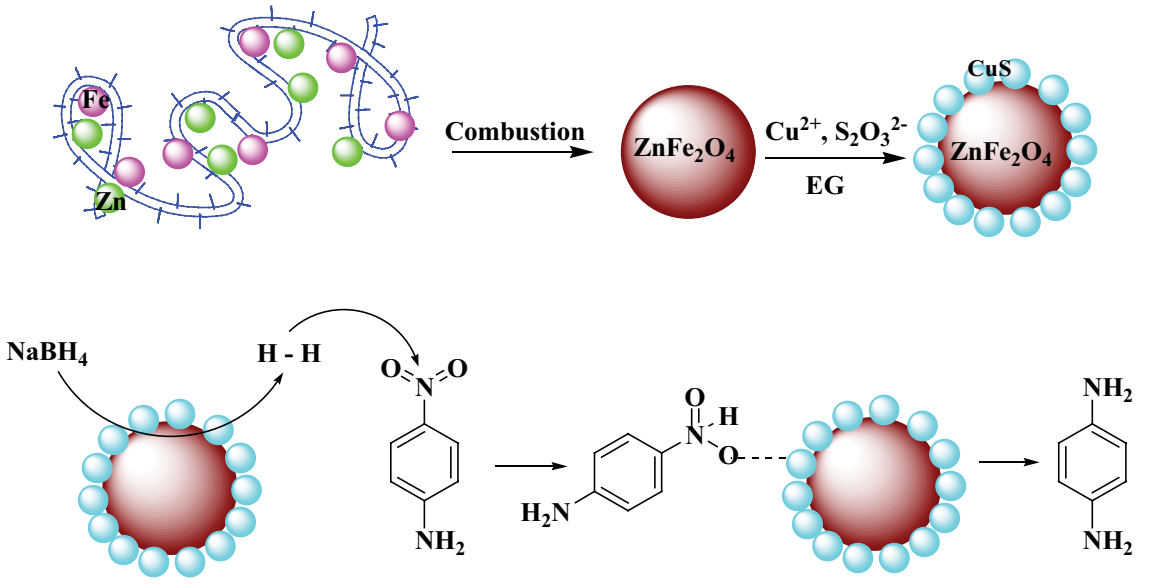

Fig. 3. A schematic illustration of nanocomposite preparation and nitro reduction.

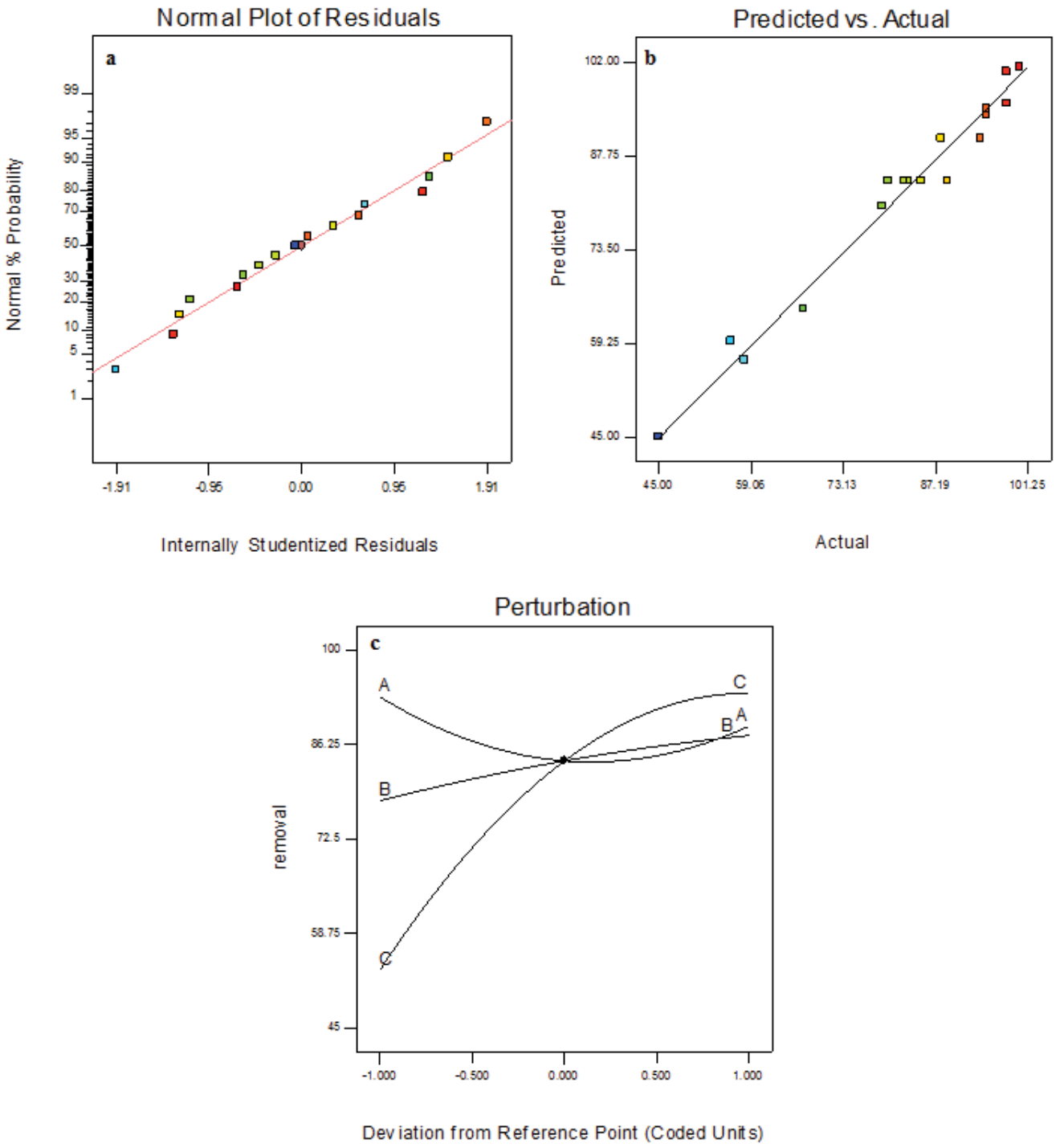

Fig. 4. Normal probability plot (a), predicted removal percentage versus actual (b), and perturbation plot of MB adsorption by the sorbent (c).

adsorption–complexation reaction in the adsorption process is shown as follow:

$$Q_e = K_f C_e^{1/n} \tag{10}$$

where n and K_f are the Freundlich coefficient [50,51]. The values of n between 1 and 10 (i.e., $1/n$ <1) represent a favorable sorption moreover the model is linear if $1/n$ = 1 and, as $1/n$ decreases, the isotherm becomes more nonlinear [52]. Results at Table 2 show that the value of n is 2.8 and confirmed the sorption is favorable. Nonlinear Langmuir adsorption isotherm is shown as follows:

$$Q_e = \frac{\left(bQ_m C_e\right)}{1 + bC_e} \tag{11}$$

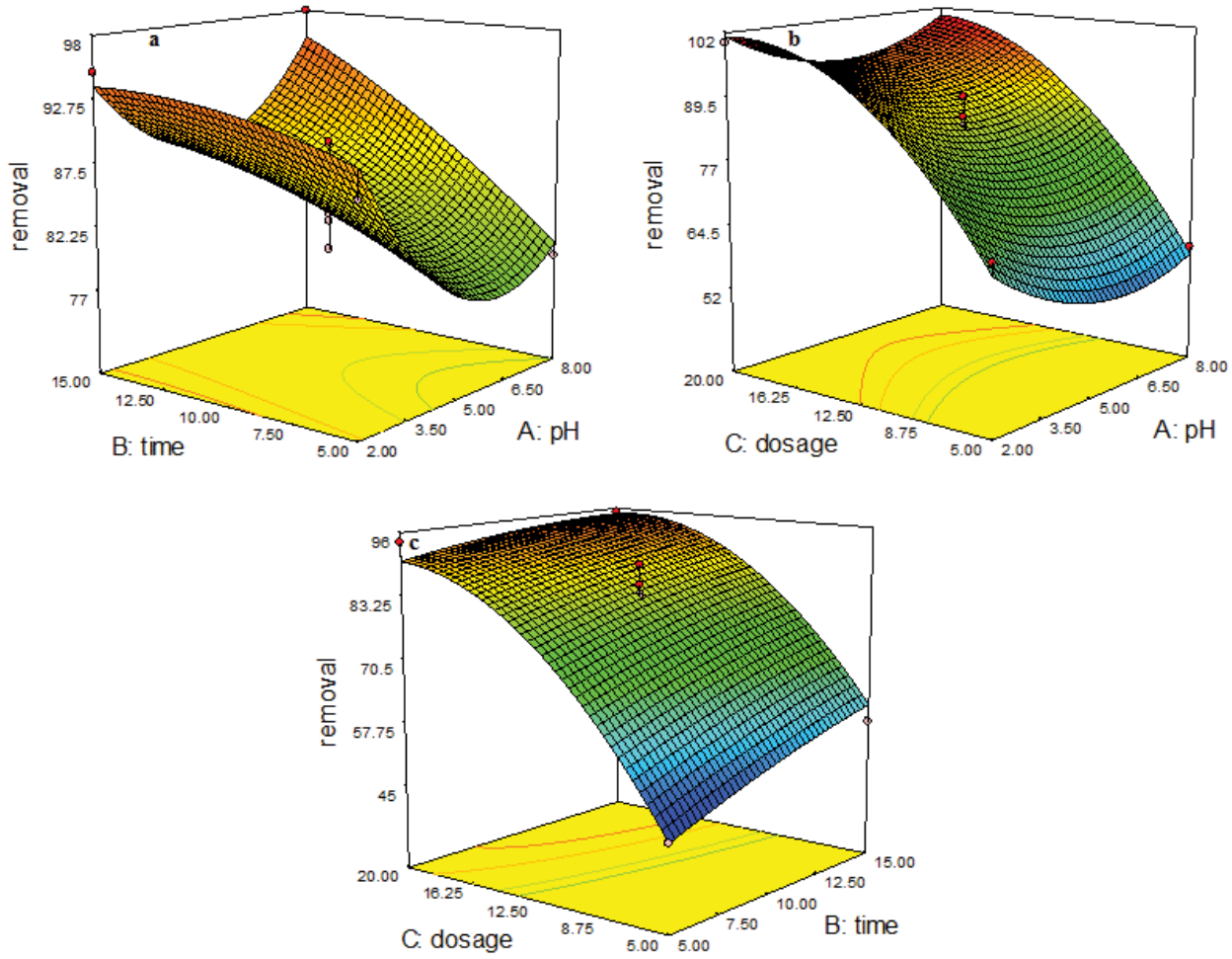

Fig. 5. A typical 3D plots of time – pH (a), dosage – pH (b) and dosage-time (c) for MB adsorption by the sorbent.

Table 2
Analysis of variance (ANOVA) for MB adsorption

Source	Sum of squares	df	Mean square	*F*-value	*P*-value prob > *F*	
Model	4,170.81	9	463.42	32.05	< 0.0001	Significant
A-pH	36.13	1	36.13	2.50	0.1580	
B-Time	180.50	1	180.50	12.48	0.0096	
C-Dosage	3,240.13	1	3,240.13	224.10	< 0.0001	
AB	36.00	1	36.00	2.49	0.1586	
AC	12.25	1	12.25	0.85	0.3879	
BC	25.00	1	25.00	1.73	0.2300	
A^2	217.30	1	217.30	15.03	0.0061	
B^2	4.70	1	4.70	0.33	0.5831	
C^2	448.08	1	448.08	30.99	0.0008	
Residual	101.21	7	14.46			
Lack of fit	55.75	3	18.58	1.64	0.3157	Not significant
Pure error	45.46	4	11.36			
Cor total	4,272.02	16				

where Q_e is the amount of MB adsorbed per unit mass of the sorbent (mg g^{-1}) and C_e is the amount of MB in the liquid phase at equilibrium (mg L^{-1}). The Q_m is the maximum adsorption capacity, and b is the Langmuir coefficient [53–55].

According to results in Table 2, both Langmuir and Freundlich models showed good linearity ($R^2 > 0.9$) as a result, some of the squared residual (RSS) was employed to evaluate the accuracy of the isotherm models [56].

$$\mathrm{RSS} = \sum \left(Q_{\exp} - Q_c\right)^2 \quad (12)$$

where $Q_{\exp}$ and Q_c are the experimental data and the calculated from the nonlinear model. According to the results (Table 3 and Fig. 6(b)), the R^2 value for the nonlinear Freundlich model is 0.94. Moreover, relative to the Langmuir model, the Freundlich model has a lower RSS value and reveals that this model can better describe adsorption behavior of MB.

3.3.2. Desorption and reusability

To make the sorption process more economical it is necessary to desorb of the target analyte from the sorbent surface hence different eluents were examined. It was observed that elution with the use of methanol, acetone, and methanol-acetone (1:1) release of MB were 40%, 60%, and 98%, respectively. Moreover, in order to evaluate the reusability of the sorbent, it was subjected to several adsorptions–desorption process. It was found that after three cycles of sorption and desorption, the efficiency was 95%, 92%, and 85% which confirm the efficiency of the nanohybrid as a regenerable adsorbent.

3.3.3. Comparison with other methods

The catalytic activity of $ZnFe_2O_4$@CuS for nitro reduction is compared with some catalysts and the results are

Table 3
The data of isotherm models for MB adsorption using $ZnFe_2O_4$@CuS

Model	Coefficient	
	Q_m (mg g^{-1})	26
	R^2	0.90
	b	1.00
Langmuir	RSS	280
	n	2.80
	K_f	11.98
Freundlich	R^2	0.94
	RSS	188

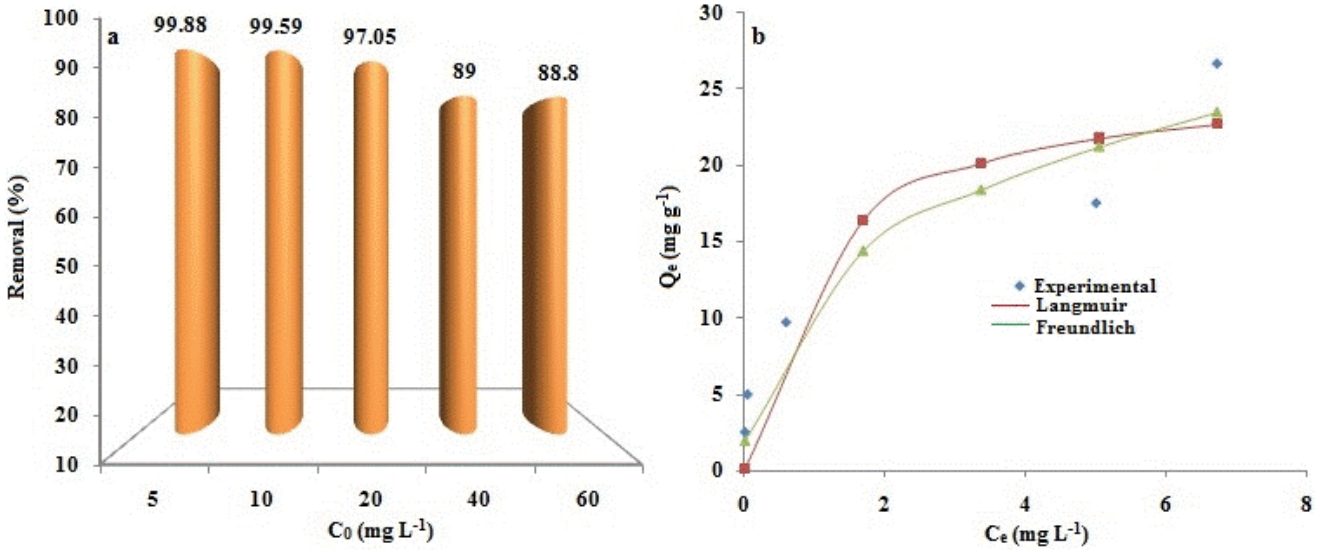

Fig. 6. Relation between MB concentration and removal efficiency (a), a typical experimental and nonlinear isotherm models (b).

Table 4
Comparison of catalyst performance with other methods for nitro reduction

Catalyst	Reducing time (min)	Condition	Ref.
Tetramethyldisiloxane $Fe(acac)_3$	24h	$Fe(acac)_3$ (10 mol%), 60°C	[1]
Cu-Nano-ZSM-5	120	$NaBH_4$ (5 equiv), 40°C	[2]
Soapnut Shells Au NPs	59	$NaBH_4$ (10 equiv), rt	[3]
Fe_3O_4 supported Pd	1	$NaBH_4$ (75 equiv), rt	[4]
Ag-Sulfydryl-Poly(glycidyl methacrylate)	13	$NaBH_4$ (3,000 equiv), rt	[5]
Bismuth nanoparticle	2	$NaBH_4$ (700 equiv), 68°C	[6]
$ZnFe_2O_4$@CuS	3	$NaBH_4$, (15 equiv), 60°C	This work

Table 5
Comparison the MB adsorption property of prepared material with some sorbents

Adsorbent	Maximum capacity (mg g^{-1})	Equilibrium time (min)	Ref.
$ZnO/ZnFe_2O_4$	37.27	0.5	[29]
Polydopamine-microspheres	88.89	80	[30]
Eucalyptus sawdust-acetic acid	29.94	120	[31]
Coir pith carbon	5.87	100	[32]
Wheat shells	16.56	75	[33]
Aleurites Moluccana	178	60	[34]
GO/calcium alginate	181.81	420	[36]
Fe_3O_4-graphene@ SiO_2	139.64	120	[37]
$ZnFe_2O_4$	12	10	This work
$ZnFe_2O_4$@CuS	26	10	This work

depicted in Table 4. The catalyst preparation is simple and cost-effective. The catalyst can reduce a nitro-compound in a few minutes moreover; this catalytic system is economic due to the absence of high-cost noble metals. A comparative study of MB adsorption with $ZnFe_2O_4$ and some previously reported ones is presented in Table 5. It was found that MB adsorption capacity was 12 mg g^{-1} using $ZnFe_2O_4$ as adsorbent which increased to 26 mg g^{-1} after preparing its composite with CuS. MB adsorption onto $ZnFe_2O_4$ is owing to hydrogen bonding reaction between oxy/hydroxy functional groups of dye and the sorbent. After growth of CuS on the $ZnFe_2O_4$ surface, a new adsorption site of –C–S was added to the sorbent increases adsorption efficiency. In comparing with other methods; the presented method showed a fast equilibrium time for MB adsorption furthermore, it shows a satisfactory adsorption capacity.

4. Conclusions

A fast solid state combustion route, as well as facial polyol route, was used for $ZnFe_2O_4$ synthesis and preparing $ZnFe_2O_4$@CuS composite for nitro reduction and MB adsorption. The nanocomposite was applied as a magnetic separable catalyst for a rapid reduction of nitroaniline to phenylenediamine. The catalytic reaction was assisted by $NaBH_4$ as a hydrogen source. Moreover, MB adsorption property of the nanocomposite was investigated by RSM. The magnetic nanocomposite shows fast catalytic and adsorption characteristic with good adsorption capacity. Isotherm study revealed that the adsorption process followed the multilayer Freundlich adsorption model. Moreover, the method represents good reusability after three cycles of sorption and desorption.

References

[1] M. Saranya, A. Nirmala Grace, Hydrothermal synthesis of CuS nanostructures with different morphology, J. Nano Res., 18–19 (2012) 43–51.

[2] X.-H. Guan, L. Yang, X. Guan, G.-S. Wang, Synthesis of a flower-like CuS/ZnS nanocomposite decorated on reduced graphene oxide and its photocatalytic performance, RSC Adv., 5 (2015) 36185–36191.

[3] L.J. Zhang, T.F. Xie, D.J. Wang, S. Li, L.L. Wang, L.P. Chen, Y.C. Lu, Noble-metal-free CuS/CdS composites for photocatalytic H_2 evolution and its photogenerated charge transfer properties, Int. J. Hydrogen Energy, 38 (2013) 11811–11817.

[4] H.S. Kim, D. Kim, B.S. Kwak, G.B. Han, M.H. Um, M. Kang, Synthesis of magnetically separable core at shell structured $NiFe_2O_4$ at TiO_2 nanomaterial and its use for photocatalytic hydrogen production by methanol/water splitting, Chem. Eng. J., 243 (2014) 272–279.

[5] L. Chen, X. Li, Y. Wang, C. Gao, H. Zhang, B. Zhao, F. Teng, J. Zhou, Z. Zhang, X. Pan, E. Xie, Low-temperature synthesis of tin dioxide hollow nanospheres and their potential applications in dye-sensitized solar cells and photoelectrochemical type self-powered ultraviolet photodetectors, J. Power Sources., 272 (2014) 886–894.

[6] K.J. Huang, J.Z. Zhang, Y. Fan, One-step solvothermal synthesis of different morphologies CuS nanosheets compared as supercapacitor electrode materials, J. Alloys Compd., 625 (2015) 158–163.

[7] Y. He, X. Yu, X. Zhao, Synthesis of hollow CuS nanostructured microspheres with novel surface morphologies, Mater. Lett., 61 (2007) 3014–3016.

[8] S.-W. Hsu, W. Bryks, A.R. Tao, Effects of carrier density and shape on the localized surface plasmon resonances of $Cu_{2-x}S$ nanodisks, Chem. Mater., 24 (2012) 3765–3771.

[9] M. Nafees, S. Ali, K. Rasheed, S. Idrees, The novel and economical way to synthesize CuS nanomaterial of different morphologies by aqueous medium employing microwaves irradiation, Appl. Nanosci., 2 (2011) 157–162.

[10] G.R. Chaudhary, P. Bansal, S.K. Mehta, Recyclable CuS quantum dots as heterogeneous catalyst for Biginelli reaction under solvent free conditions, Chem. Eng. J., 243 (2014) 217–224.

[11] Y. Li, H. Wang, X. Li, T. Chen, D. Zhao, CuS/Fe: a novel and highly efficient catalyst system for coupling reaction of aryl halides with diaryl diselenides, Tetrahedron, 66 (2010) 8583–8586.

[12] P. Bansal, G.R. Chaudhary, N. Kaur, S.K. Mehta, An efficient and green synthesis of xanthene derivatives using CuS quantum dots as a heterogeneous and reusable catalyst under solvent free conditions, RSC Adv., 5 (2015) 8205–8209.

[13] R. Kaplánek, V. Krchňák, Fast and effective reduction of nitroarenes by sodium dithionite under PTC conditions: application in solid-phase synthesis, Tetrahedron Lett., 54 (2013) 2600–2603.

[14] L. Pehlivan, E. Métay, S. Laval, W. Dayoub, P. Demonchaux, G. Mignani, M. Lemaire, Alternative method for the reduction of aromatic nitro to amine using TMDS-iron catalyst system, Tetrahedron, 67 (2011) 1971–1976.

[15] L. Pehlivan, E. Métay, S. Laval, W. Dayoub, P. Demonchaux, G. Mignani, M. Lemaire, Iron-catalyzed selective reduction of nitro compounds to amines, Tetrahedron Lett., 51 (2010) 1939–1941.

[16] B. Kaur, M. Tumma, R. Srivastava, Transition-metal-exchanged nanocrystalline ZSM-5 and metal-oxide-incorporated SBA-15 catalyzed reduction of nitroaromatics, Ind. Eng. Chem. Res., 52 (2013) 11479–11487.

[17] V. Reddy, R.S. Torati, S. Oh, C. Kim, Biosynthesis of gold nanoparticles assisted by Sapindus mukorossi Gaertn. Fruit pericarp and their catalytic application for the reduction of p-nitroaniline, Ind. Eng. Chem. Res., 52 (2013) 556–564.

[18] A. Baykal, E. Karaoglu, H. Sözeri, E. Uysal, M.S. Toprak, Synthesis and characterization of high catalytic activity magnetic Fe_3O_4 supported Pd nanocatalyst, J. Supercond. Novel Magn., 26 (2013) 165–171.
[19] W. Zhang, Y. Sun, L. Zhang, In situ synthesis of monodisperse silver nanoparticles on sulfhydryl-functionalized poly(glycidyl methacrylate) microspheres for catalytic reduction of 4-nitrophenol, Ind. Eng. Chem. Res., 54 (2015) 6480–6488.
[20] F. Xia, X. Xu, X. Li, L. Zhang, L. Zhang, H. Qiu, W. Wang, Y. Liu, J. Gao, Preparation of bismuth nanoparticles in aqueous solution and its catalytic performance for the reduction of 4-nitrophenol, Ind. Eng. Chem.Res., 53 (2014) 10576–10582.
[21] S. Yoo, S. Lee, Reduction of organic compounds with sodium borohydride-copper(II) sulfate system, Synlett, 1990 (1990) 419–420.
[22] S. Pina, D.M. Cedillo, C. Tamez, N. Izquierdo, J.G. Parsons, J.J. Gutierrez, Reduction of nitrobenzene derivatives using sodium borohydride and transition metal sulfides, Tetrahedron Lett., 55 (2014) 5468–5470.
[23] W. Xu, S. Zhu, Y. Liang, Z. Li, Z. Cui, X. Yang, Nanoporous CuS with excellent photocatalytic property, Sci. Rep., 5 (2015) 1–11.
[24] M.J. Pirouz, M.H. Beyki, F. Shemirani, Anhydride functionalised calcium ferrite nanoparticles: a new selective magnetic material for enrichment of lead ions from water and food samples, Food Chem., 170 (2015) 131–137.
[25] J. Zhang, J.M. Song, H.L. Niu, C.J. Mao, S.Y. Zhang, Y.H. Shen, ZnFe2O4 nanoparticles: synthesis, characterization, and enhanced gas sensing property for acetone, Sens. Actuators, B, 221 (2015) 55–62.
[26] A. Khazaei, A. Ranjbaran, F. Abbasi, M. Khazaei, A.R. Moosavi-Zare, Synthesis, characterization and application of $ZnFe_2O_4$ nanoparticles as a heterogeneous ditopic catalyst for the synthesis of pyrano[2,3-d] pyrimidines, RSC Adv., 5 (2015) 13643–13647.
[27] S. Debnath, J. Kitinya, M.S. Onyango, Removal of Congo red from aqueous solution by two variants of calcium and iron based mixed oxide nano-particle agglomerates, J. Ind. Eng. Chem., 20 (2014) 2119–2129.
[28] I. Tamiolakis, S. Fountoulaki, N. Vordos, I.N. Lykakis, G.S. Armatas, Mesoporous Au-TiO_2 nanoparticle assemblies as efficient catalysts for the chemoselective reduction of nitro compounds, J. Mater. Chem. A, 1 (2013) 14311–14319.
[29] J. Feng, Y. Wang, L. Zou, B. Li, X. He, Y. Ren, Y. Lv, Z. Fan, Synthesis of magnetic ZnO/$ZnFe_2O_4$ by a microwave combustion method, and its high rate of adsorption of methylene blue, J. Colloid Interface Sci., 438 (2015) 318–322.
[30] J. Fu, Z. Chen, M. Wang, S. Liu, J. Zhang, J. Zhang, R. Han, Q. Xu, Adsorption of methylene blue by a high-efficiency adsorbent (polydopamine microspheres): kinetics, isotherm, thermodynamics and mechanism analysis, Chem. Eng. J., 259 (2014) 53–61.
[31] L. Sun, D. Chen, S. Wan, Z. Yu, Performance, kinetics, and equilibrium of methylene blue adsorption on biochar derived from eucalyptus saw dust modified with citric, tartaric, and acetic acids, Biores. Technol., 198 (2015) 300–308.
[32] D. Kavitha, C. Namasivayam, Experimental and kinetic studies on methylene blue adsorption by coir pith carbon, Biores. Technol., 98 (2007) 14–21.
[33] Y. Bulut, H. Ayd, A kinetics and thermodynamics study of methylene blue adsorption on wheat shells, Desalination, 194 (2006) 259–267.
[34] D.L. Postai, C.A. Demarchi, F. Zanatta, A. Rodrigues, D. Caroline, C. Melo, Adsorption of rhodamine B and methylene blue dyes using waste of seeds of Aleurites Moluccana, a low cost adsorbent, Alexandria Eng. J., 55 (2016) 1713–1723.
[35] Z. Jian, P. Qingwei, N. Meihong, S. Haiqiang, L. Na, Kinetics and equilibrium studies from the methylene blue adsorption on diatomite treated with sodium hydroxide, Appl. Clay Sci., 84 (2013) 12–16.
[36] Y. Li, Q. Du, T. Liu, J. Sun, Y. Wang, S. Wu, Z. Wang, Y. Xia, L. Xia, Methylene blue adsorption on graphene oxide/calcium alginate composites, Carbohydr. Polym., 95 (2013) 501–507.
[37] X. Wu, Y. Shi, S. Zhong, H. Lin, J. Chen, Facile synthesis of Fe_3O_4-graphene @ mesoporous SiO_2 nanocomposites for efficient removal of Methylene Blue, Appl. Surf. Sci., 378 (2016) 80–86.
[38] X. Liu, Y. Zhou, W. Nie, L. Song, Fabrication of hydrogel of hydroxypropyl cellulose (HPC) composited with graphene oxide and its application for methylene blue removal, J. Mater. Sci., 50 (2015) 6113–6123.
[39] C. Yao, Q. Zeng, G.F. Goya, T. Torres, J. Liu, H. Wu, M. Ge, Y. Zeng, Y. Wang, J.Z. Jiang, $ZnFe_2O_4$ nanocrystals: synthesis and magnetic properties, J. Phys. Chem. C, 111 (2007) 12274–12278.
[40] Z.H. Wang, D.Y. Geng, Y.J. Zhang, Z.D. Zhang, CuS:Ni flowerlike morphologies synthesized by the solvothermal route, Mater. Chem. Phys., 122 (2010) 241–245.
[41] F. Li, J. Wu, Q. Qin, Z. Li, X. Huang, Controllable synthesis, optical and photocatalytic properties of CuS nanomaterials with hierarchical structures, Powder Technol., 198 (2010) 267–274.
[42] A. Yan, X. Liu, G. Qiu, H. Wu, R. Yi, N. Zhang, J. Xu, Solvothermal synthesis and characterization of size-controlled Fe_3O_4 nanoparticles, J. Alloys Compd., 458 (2008) 487–491.
[43] W. Zhang, F. Shen, R. Hong, Solvothermal synthesis of magnetic Fe_3O_4 microparticles via self-assembly of Fe3O4 nanoparticles, Particuology, 9 (2011) 179–186.
[44] S. Wunder, F. Polzer, Y. Lu, Y. Mei, M. Ballauff, Kinetic analysis of catalytic reduction of 4-nitrophenol by metallic nanoparticles immobilized in spherical polyelectrolyte brushes, J. Phys. Chem. C, 114 (2010) 8814–8820.
[45] S. Özkar, M. Zahmakiran, Hydrogen generation from hydrolysis of sodium borohydride using Ru(0) nanoclusters as catalyst, J. Alloys Compd., 404–406 (2005) 728–731.
[46] M.H. Beyki, M. Bayat, F. Shemirani, Fabrication of core–shell structured magnetic nanocellulose base polymeric ionic liquid for effective biosorption of Congo red dye, Biores. Technol., 218 (2016) 326–334.
[47] M. Iqbal, N. Iqbal, I. Ahmad, N. Ahmad, M. Zahid, Response surface methodology application in optimization of cadmium adsorption by shoe waste: a good option of waste mitigation by waste, Ecol. Eng., 88 (2016) 265–275.
[48] M.K. Nduna, A.E. Lewis, P. Nortier, A model for the zeta potential of copper sulphide, Colloids Surf., A, 441 (2014) 643–652.
[49] L. Su, J. Feng, X. Zhou, C. Ren, H. Li, X. Chen, Colorimetric detection of urine glucose based $ZnFe_2O_4$ magnetic nanoparticles, Anal. Chem., 84 (2012) 5753–5758.
[50] Y. Ge, Q. Song, Z. Li, A Mannich base biosorbent derived from alkaline lignin for lead removal from aqueous solution, J. Ind. Eng. Chem., 23 (2015) 228–234.
[51] Q. Wang, J. Feng, L. Ma, W. Wei, J. Xie, C. Xia, J. Zhu, D. Jiang, Synthesis, characterization, and adsorption properties of silica aerogels crosslinked with diisocyanate under ambient drying, J. Mater. Sci., 51 (2016) 9472–9483.
[52] T.K. Naiya, A.K. Bhattacharya, S.K. Das, Clarified sludge (basic oxygen furnace sludge) – an adsorbent for removal of Pb(II) from aqueous solutions – kinetics, thermodynamics and desorption studies, J. Hazard. Mater., 170 (2009) 252–262.
[53] T.S. Anirudhan, F. Shainy, Adsorption behaviour of 2-mercaptobenzamide modified itaconic acid-grafted-magnetite nanocellulose composite for cadmium (II) from aqueous solutions, J. Ind. Eng. Chem., 32 (2015) 157–166.
[54] E. Igberase, P. Osifo, Equilibrium, kinetic, thermodynamic and desorption studies of cadmium and lead by polyaniline grafted cross-linked chitosan beads from aqueous solution, J. Ind. Eng. Chem., 26 (2015) 340–347.
[55] Q. Huang, M. Liu, R. Guo, L. Mao, Q. Wan, G. Zeng, H. Huang, F. Deng, X. Zhang, Y. Wei, Facile synthesis and characterization of poly(levodopa)-modified silica nanocomposites via self-polymerization of levodopa and their adsorption behavior toward Cu^{2+}, J. Mater. Sci., 51 (2016) 9625–9637.
[56] M.H. Beyki Shemirani, F. Shemirani, Dual application of facilely synthesized Fe3O4 nanoparticles: fast reduction of nitro compound and preparation of magnetic polyphenylthiourea nanocomposite for efficient adsorption of lead ions, RSC Adv., 5 (2015) 22224–22233.